

Journal of Materials Chemistry A

Accepted Manuscript



This is an *Accepted Manuscript*, which has been through the Royal Society of Chemistry peer review process and has been accepted for publication.

Accepted Manuscripts are published online shortly after acceptance, before technical editing, formatting and proof reading. Using this free service, authors can make their results available to the community, in citable form, before we publish the edited article. We will replace this *Accepted Manuscript* with the edited and formatted *Advance Article* as soon as it is available.

You can find more information about *Accepted Manuscripts* in the [Information for Authors](#).

Please note that technical editing may introduce minor changes to the text and/or graphics, which may alter content. The journal's standard [Terms & Conditions](#) and the [Ethical guidelines](#) still apply. In no event shall the Royal Society of Chemistry be held responsible for any errors or omissions in this *Accepted Manuscript* or any consequences arising from the use of any information it contains.

**Gel Electrolytes Based on an Ether-Abundant Polymeric Framework
for High-Rate and Long-Cycle-Life Lithium Ion Batteries**

Li-Yu Huang,¹ You-Chao Shih,¹ Shih-Hong Wang,¹ Ping-Lin Kuo,¹ and Hsisheng
Teng^{1,2,*}

¹Department of Chemical Engineering and Research Center for Energy
Technology and Strategy, National Cheng Kung University, Tainan 70101, Taiwan

²Center for Micro/Nano Science and Technology, National Cheng Kung
University, Tainan 70101, Taiwan

*To whom correspondenc should be addressed. E-mail: hteng@mail.ncku.edu.tw, Tel:
886-6-2385371, Fax:886-6-2344496

Huang *et al.*²**Abstract**

This study reports a gel polymer electrolyte (GPE) that is synthesized using a poly(ethylene oxide)-co-poly(propylene oxide) copolymer blending diglycidyl ether of bisphenol-A (i.e., P(PO-*co*-EO)) as a host swelled by a liquid electrolyte (LE) of 1 M LiPF₆ in carbonate solvents. The P(PO-*co*-EO) copolymer in the GPE contains a high concentration of ether groups to coordinate solvent molecules and solvated Li⁺ ions for achieving high ionic conductivity (3.8×10^{-3} S cm⁻¹ at 30 °C), and exhibits an excellent Li⁺ transference number of 0.7. The GPE is assembled in a full-cell lithium ion battery (LIB) consisting of an LiFePO₄ cathode and a graphite anode, and the copolymer network facilitates ion motion to reduce the equivalent series resistance by 50% and increase specific power by two times relative to the performance of an LIB assembled using the LE. This GPE-based LIB exhibits a capacity of 125 mAh g⁻¹ at 0.1 C and is able to deliver 22 mAh g⁻¹ of electricity at 15 C. This LIB exhibits superior stability; it presents negligible capacity decay after 200 charge–discharge cycles at 1 C, and exhibits 77% capacity retention after 450 cycles. The distinctive merit of the GPE film is its mechanical integrity, which ensures that the roll-to-roll assembly of GPE-based LIBs is readily scalable to industrial levels.

Keywords: gel polymer electrolyte; lithium ion battery; poly(ethylene oxide); LiFePO₄ electrode; graphite electrode

1. Introduction

Over the past few decades, concerns regarding the safety and cycle-life of electrochemical energy-delivering devices such as lithium ion batteries (LIBs), solar cells, and capacitors have motivated research on gel polymer electrolytes (GPEs),¹⁻⁵ which comprise a polymeric framework that entraps organic solvents and supports electrolytic salts. GPEs are being developed for device applications that require high power and low energy loss. LIBs consisting of two electrodes made of distinct materials present a challenge in ensuring compatibility between developed GPEs and electrodes.⁶ Most previous efforts have focused on GPE performance in half-cell assemblies, whereas only a limited number of studies have explored structural designs for GPEs that can fulfill the strict requirements for operating full cells and offer a high-rate performance and long cycle life.

Commonly used polymer hosts for GPEs include poly(ethylene oxide) (PEO),⁷⁻¹¹ poly(vinylidene fluoride) (PVDF),^{14,15} poly(vinylidene fluoride-co-hexafluoropropylene),¹⁶⁻¹⁸ poly(urethane),¹⁹ poly(acrylonitrile),²⁰ and poly(methyl methacrylate).²¹⁻²³ Among these polymers, PEO has attracted substantial attention because its ether linkages exhibit favorable affinity with cations and solvents. However, its strong crystallization tendency, which impedes ionic motion in the resulting GPEs, and poor mechanical integrity restrict its practical application.²⁴⁻²⁶ To enhance the ionic conductivity and mechanical strength of PEO-based GPEs, fillers have been added, blending or grafting with other polymers has been conducted, and porous polyolefin separators have been incorporated in previous studies.²⁷⁻³¹ Polypropylene oxide (PPO), which effectively suppresses PEO crystallization by using its methyl side chains and provides a hydrophobic property that is complementary to hydrophilic PEO,³²⁻³⁵ is an excellent implant choice for improving

Huang *et al.*⁴

the ionic conductivity of PEO and its affinity with electrodes. Regarding mechanical strength, bisphenol-containing ether linkages can improve the structural integrity of PEO and exhibit high affinity with electrolytes.^{36,37}

Lithium ions are the only charge carrier involved in charge storage in both the cathode and anode of LIBs. The transport of counter anions during charge storage results in electrode polarization, which considerably deteriorates the cycle life and rate performance of batteries.^{38–40} The purpose of this study was to design GPEs that facilitate Li^+ ion transport while maintaining stationary counter anions. In addition to suppressing anion motion, preventing extensive interaction between solvent molecules and the carbon anode is another objective of designing GPEs for creating high-performance LIBs. This interaction induces the formation of solid-electrolyte interface (SEI) layers that affect ionic conduction and electrode capacity.^{41–44} Polymers in GPEs may form a complex with SEI layers to circumscribe further electrolyte decomposition on the anode.

In this study, a P(EO-co-PO) polymeric network was prepared using poly(ethylene glycol) diglycidyl ether (PEGDE) to construct the body frame and poly(propylene oxide) diamines as the curing agent. Blending diglycidyl ether of bisphenol-A (DGEBA) with the polymer precursors before curing enhanced the mechanical strength of the polymer. Swelling the resulting ether-abundant P(EO-co-PO) copolymer with a liquid electrolyte (LE) of 1 M LiPF_6 in carbonate solvents formed a GPE that exhibited excellent ionic conductivity, mechanical integrity, film-forming feasibility, and chemical stability. By incorporating this GPE with a graphite anode and a LiFePO_4 cathode, we developed a full-cell LIB that delivered energy at high rates ($> 15\text{ C}$) and exhibited excellent capacity retention with long-term cycling. Table 1 shows the performance comparison of the LIB developed

in this study with other reported full-cell batteries.^{8–13} The high compatibility of this GPE with both electrodes, and the large transference number of Li⁺ ions in this GPE, were primarily responsible for the outstanding performance of the resulting LIB.

2. Experimental

2.1. Synthesis of GPE films. To prepare the P(EO-*co*-PO) polymeric framework of the gel electrolyte, we blended a mixture of PEGDE (Kyoehisha) and DGEBA (Nan-Ya), which had epoxy group equivalent weights of 290 and 190 g equiv.⁻¹, respectively, with a curing agent— α,ω -diamino poly(propylene oxide) (Huntsman Jeffamine D2000) with an active hydrogen equivalent weight of 514 g equiv.⁻¹. A polymer precursor solution was formed by dissolving 0.1 g of PEGDE, 0.1 g of DGEBA, and 0.45 g of D2000 in 1 mL of dimethylacetamide (DMAC) using mechanical stirring. The solution was spread on an aluminum plate and heated at 90 °C for 8 h to evaporate the DMAC and cure the contained polymers. The resulting P(EO-*co*-PO) film was 100- μ m thick, flexible, and transparent. This film was soaked in the LE solution, which consisted of 1 M LiPF₆ dissolved ethylene carbonate/dimethyl carbonate/diethyl carbonate (EC/DMC/DEC; 1:1:1 by volume), in an argon environment to trap the solution in the polymer network and form the GPE film. The amount of trapped solution was adjusted by varying the soak time. The mass of the trapped LE was two times the P(EO-*co*-PO) film mass in the GPE. This mass ratio was obtained by pressing the LE-saturated P(EO-*co*-PO) film under a load of 9.8 N cm⁻¹ in argon by using a pneumatic flat press. We used this stabilized LE-P(EO-*co*-PO) composite film, which had a LE/ P(EO-*co*-PO) mass ratio of 2/1,

Huang *et al.*⁶

as a GPE for subsequent testing and battery assembly.

2.2. Electrode preparation and cell assembly. The LIB cathodes consisted of 80 wt% LiFePO₄ (BTR New Energy Materials), 10 wt% PVDF ($M_w = 534000 \text{ g mol}^{-1}$; Aldrich, USA), and 10 wt% super-P carbon black (Taiwan Maxwave Co.). A slurry of these materials dissolved in N-methyl pyrrolidone (NMP, Aldrich) was blade-coated on aluminum foil. After solvent evaporation, disks that were 1.3 cm in diameter were punched from the foil and dried by heating at 80 °C in a vacuum for 12 h. The cathodes were roll-pressed to improve their particulate contact and foil adhesion, and had a pressed thickness of 40–50 μm. The anode was prepared in the same manner as the cathode was prepared, and consisted of 92 wt% graphite (Long Time Technology Co.), 3 wt% PVDF, and 5 wt% super-P. Full-cell LIBs were assembled by sandwiching the GPE film between the graphite anode and LiFePO₄ cathode and then vacuum-sealing the battery in a coin cell. All cell assemblies were conducted in a glove box filled with argon gas.

2.3. Measurements. Fourier transform infrared (FTIR) spectroscopy in diffuse reflectance mode was conducted to analyze the functionalities of the P(EO-*co*-PO) film by using a Jasco FTIR-4100 spectrometer. Raman spectra of the GPE and LE specimens were recorded at room temperature by using a Bayspec Raman spectrometer with a laser line of 1064 nm. The Raman measurement resolution was 4 cm⁻¹ and the Lorentzian function was used to deconvolute the 880–950 cm⁻¹ and 700–760 cm⁻¹ bands into constituting peaks. The ionic conductivity of the GPE was analyzed at varying temperatures by conducting AC impedance spectroscopy (Zahner-Elektrok IM6e) using a sandwich-type cell consisting of two stainless-steel

electrodes. This measurement was conducted at 0 V with an AC potential amplitude of 5 mV and a frequency range of 0.1 Hz to 1 MHz. The interface resistance between the GPE and lithium metal electrode was measured using the impedance response of Li|GPE|Li cells. Charge and discharge cycling tests were conducted on full-cell LIBs between 2.0 and 3.8 V galvanostatically by using battery test equipment (Acutech System BAT-750). All electrochemical measurements were conducted at 25 °C, except for the conductivity measurements. For the purpose of comparison, the performance of the LE in swelling a membrane (Celgard M824), which was used as a separator, was also analyzed in the same manner as the GPE was analyzed.

3. Results and Discussion

3.1. Synthesis of GPEs. Ether groups in polymer chains are effective in solvating carbonate solvents and entrapping the solvent molecules in the polymeric framework.⁶ Strong solvent-entrapping ability suppresses the leakage or evaporation of solvent and creates space in GPEs to facilitate ionic motion. By contrast, commercially available separators, generally consisting of polypropylene and polyethylene that are compatible with organic solvents and have mechanical integrity, demonstrate poor ability to entrap solvent molecules.⁴⁵ In the synthesis of ether-abundant polymers, the incorporation of PEO and PPO reduces the crystallization tendency of polymer chains, and the introduction of bisphenol-A segments to the resulting P(EO-*co*-PO) improves the mechanical properties of the copolymer.²⁷ Scheme 1 depicts the structures of PEO-containing PEGDE, PPO-containing Jeffamine D2000, and bisphenol A-containing DGEBA, as well as the major linkages in the resulting

Huang *et al.*⁸

P(EO-*co*-PO) polymers. The amine groups of Jeffamine D2000 interacted with the epoxy groups of PEGDE and DGEBA to connect PEO, PPO, and bisphenol-A chains and construct a 3D network populated with ether linkages.

Fig. 1a shows a top-view photograph of a P(EO-*co*-PO) film with a diameter of approximately 1.2 cm. The film expanded to a diameter of 1.6 cm after being soaked in 1 M LiPF₆ LE for 80 min (Fig. 2b) to form a GPE film. The size increase demonstrated the strong solvent-entrapping ability of the P(EO-*co*-PO) framework. Fig. 2 shows the time course of electrolyte uptake for the P(EO-*co*-PO) film after the film was soaked in LE. The electrolyte absorption reached saturation in 30 min and the uptake amount was 3.4 times the film mass. By pressing the LE-saturated P(EO-*co*-PO) film using a load of 9.8 N cm⁻¹ in Ar, solvent leakage occurred and the film produced a stabilized LE uptake that was two times the P(EO-*co*-PO) film mass.⁴⁶ We used the stabilized LE-P(EO-*co*-PO) composite film as a GPE for subsequent analysis and cell assembly. The P(EO-*co*-PO) film that contained ether groups entrapped solvent molecules to form a 3D cross-linked network, which served as the continuous solid phase of the gel system. The ability of polymer gellation accounts for the high LE capacity of the polymer host in gel electrolytes. The GPE film was highly flexible and exhibited structural integrity. Fig. 1c shows that the GPE film regained its original configuration after extensive bending and twisting treatments. This flexibility assures close contact between the GPE film and electrodes.

3.2. Chemical Characterization of the GPE. Fig. 3 shows the FTIR spectroscopic analysis of the functional groups of the P(EO-*co*-PO) film. The spectrum exhibited the characteristic stretching vibration of alkyl groups near 2850–2960 cm⁻¹, and the bending signals of –CH₂– and –CH₃ at 1460 and 1380 cm⁻¹, respectively.^{47,48} The

C–O–C stretching of PPO and PEO signaled peaks at 1110 and 1070 cm^{-1} , respectively. The aromatic components of DGEBA signaled peaks at 1610 and 1510 cm^{-1} for the C–C stretching of benzene rings and 1250 and 830 cm^{-1} for the aromatic ethers.^{49,50} The 900 cm^{-1} peak for epoxy stretching did not appear in the spectrum, whereas the 930 cm^{-1} peak for C–N bonding was present.⁵¹ The presence of C–N at the expense of epoxy loss indicated the bridging reactions between the amine groups in D2000 with the epoxy groups in PEGDE and DGEBA to form a cross-linked framework in the P(EO-co-PO) film (Scheme 1).

Fig. 4 shows a comparison of the GPE and LE Raman spectra. The strong band ranging from 700–760 cm^{-1} encompasses the ring bending modes of free EC and Li^+ -associated EC (i.e., Li^+ -EC) at 718 and 726 cm^{-1} , respectively, as well as the symmetric vibration of free PF_6^- at 741 cm^{-1} .⁵² The 880–950 cm^{-1} region includes contributions from the symmetric ring breathing of free EC and Li^+ -EC at 894 and 902 cm^{-1} , respectively, as well as the O–CH₃ stretching of free DEC/DMC and Li^+ -DEC/DMC at 915 and 937 cm^{-1} , respectively.⁵² The absence of an Li^+PF_6^- contact ion peak at 951 cm^{-1} indicates the complete dissociation of the LiPF_6 salt in both electrolytes, which is attributable to the high dielectric constant of EC (approximately 90).^{53–56} Fig. 5a shows the magnification of the 700–760 cm^{-1} band, which was deconvoluted into constituting peaks (the dotted lines) by using Lorentzian curve fitting. The GPE exhibited a lower intensity for free EC (peak 718 cm^{-1}) than the LE did, indicating the association of EC molecules with the polymer chains in the GPE. The polymer also solvated Li^+ ions and resulted in a suppressed Li^+ -EC signal (726 cm^{-1}) compared with that of EC. The solvation of Li^+ ions by polymer chains promoted the transport of Li^+ ions through the segmental motion of these polymer chains.

Huang *et al.*¹⁰

Fig. 5b shows the magnification and peak deconvolution of the Raman 880–950 cm^{-1} region. The signal of free DEC/DMC in the LE was much lower than that of Li^+ -DEC/DMC, indicating that most DEC/DMC molecules interacted with Li^+ ions or the polymer chains. The GPE spectra showed the disappearance of the Li^+ -DEC/DMC peak, indicating the association of Li^+ -DEC/DMC complexes with the polymer chains. The EC-related peaks (894 and 902 cm^{-1}) indicated that the polymer chains in the GPE interacted with Li^+ -EC complexes to suppress the Li^+ -EC signal. The results shown in Fig. 5b demonstrated the intensive interaction between solvent-solvated Li^+ ions and polymer chains. This interaction explains the high solution-entrapping ability of the P(EO-*co*-PO) framework and the high mobility of Li^+ cations, relative to that of the PF_6^- anions, in the GPE film (see the results shown later).

3.3. Ionic Conductivity. The AC impedance method was used to analyze the ionic conductivity of the GPE and LE at temperatures ranging from $-20\text{ }^\circ\text{C}$ to $80\text{ }^\circ\text{C}$ (see Fig. S1 of the ESI[†]). The GPE impedance curves were less inclined than those of the LE, indicating that the GPE was more stable and less prone to charge transfer at the electrode interface than the LE was. The ionic conductivity of the electrolytes was determined using $\sigma = R_1^{-1} \times S^{-1} \times d$, where σ represents the ionic conductivity, R_1 is the intercept at the real axis in the impedance Nyquist plot, S is the geometric area of the electrolyte-electrode interface, and d is the distance between the two electrodes.⁵⁷

Fig. 6 presents the GPE and LE ionic conductivities at varying temperatures in an Arrhenius plot. The GPE was more ion-conductive than the LE was. For example, at $30\text{ }^\circ\text{C}$, the ionic conductivity values of the GPE and LE were 3.82×10^{-3} and $4.3 \times 10^{-4}\text{ S cm}^{-1}$, respectively. The GPE comprises a swollen amorphous polymer framework and a liquid phase in the free volume, which both provide paths for ion

conduction.^{58,59} The high conductivity of the GPE can be attributed to the large free volume in the GPE resulting from solution entrapping. The transport of ions in the LE was hindered by the separator membrane, which was not designed to entrap electrolyte solutions. Fig. 6 shows that the curve of the GPE did not fit the Arrhenius equation ($\sigma = A \exp(-E_a/T)$, where A is a constant and E_a is the activation energy), whereas it fit the Vogel–Tamman–Fulcher (VTF) equation for gel electrolytes ($\sigma = AT^{-1/2} \exp[-E_a/(T - T_0)]$, where the T_0 value was 203 K, which was close to the glass-transition temperature of the polymer matrix). The fit to the VTF equation confirmed that ion conduction in the GPE was related to both free-volume transport and polymer segmental motion.⁶⁰ The temperature dependence of ionic conductivity in EC obeyed the Arrhenius equation, but exhibited demarcation near 20–30 °C that might be caused by EC crystallization during the cooling process, which facilitated a rapid decrease in ionic conductivity. The large E_a value in the low-temperature regime indicated that EC crystallization influenced the temperature dependence of conductivity. Comparing the GPE and LE data revealed that the functional groups in the GPE effectively dissociated the EC-molecule clusters to avoid crystallization.

3.4. Interfacial Charge Transfer. Lithium metal generally reacts with the carbonate molecules in electrolytes to form passivation (or SEI) layers that affect Li^+ -ion transfer at the electrode/electrolyte interface.^{61–63} A thick SEI layer obstructs Li^+ -ion movement at the electrode-electrolyte interface. This interfacial resistance often increases with storage time because the thickness gradually increases.^{61,62} We analyzed the electrolyte/Li-metal interface with AC impedance by using sandwich-type Li|electrolyte|Li cells at various storage times. Fig. 7 (a and b) shows the impedance data of the cells sandwiching the GPE and LE. The inset of Fig. 7a

Huang *et al.*¹²

shows an equivalent circuit model that simulates the bulk solution resistance (R_b), interface resistance (R_{int}), interface capacitance (C_{int}), and Warburg impedance (Z_w) elements of the cells.⁶⁴ The distance between the semicircle intercepts on the real axis corresponded to R_{int} , which was associated with the polarization of the electrodes, i.e., the resistance of charge transport across the passivation layers and that of the Li/Li^+ redox reaction, $\text{Li}^+ + \text{e}^- = \text{Li}$. Since the redox reaction was fast on the Li-metal surface, the semicircle associated with this charge transfer process would be negligible and merged with the semicircle associated with the passivation layers in these Li|electrolyte|Li cells. Therefore, each spectra in Fig. 7 (a and b) exhibited only one semicircle.

Fig. 7c shows the storage time dependences of R_b and R_{int} for the two cells. The R_b values were stable over time and small relative to those of R_{int} . The GPE cell produced smaller R_{int} values than those produced by the LE cell. Both electrolytes demonstrated an increase in R_{int} with time. The R_{int} value of the GPE stabilized at 74 Ω after 70 h, but that of the LE continued to increase steadily. The smaller R_{int} value of the GPE relative to that of the LE indicated that solvent molecules were stabilized by conjugating with polymer chains, thereby suppressing passivation layer growth.⁶⁵

In addition to passivation layer formation, electrode polarization resulting from counter-anion motion affects the interfacial charge transfer. A high lithium transference number (t_{Li^+}) is beneficial in eliminating polarization resistance. Electrolyte t_{Li^+} values were determined using DC polarization of the sandwich-type cell and AC impedance spectroscopic analysis.^{66–68} We applied 5 mV to the cell (Fig. 8a) and measured the initial and steady-state DC currents (I_0 and I_{ss}). Simultaneous AC impedance analysis, as shown in Fig. 8 (b and c), was used to monitor the initial and final charge-transfer resistances at the Li-metal interface, $R_{int,0}$ and $R_{int,ss}$,

respectively. Polarization caused an increase in $R_{int,ss}$. Combining the obtained parameters produced the t_{Li^+} values.

$$t_{Li^+} = \frac{I_{ss} (\Delta V - I_0 R_{int,0})}{I_0 (\Delta V - I_{ss} R_{int,ss})} \quad (1)$$

Using Equation (1), a t_{Li^+} value of 0.7 was obtained for the GPE whereas the LE had a value of only 0.4. The larger t_{Li^+} for the GPE indicated that the segmental motion of polymer chains specifically facilitated the transport of solvent-solvated Li^+ ions because of the strong Li^+ -polymer interaction, which was indicated by Raman analysis (Fig. 5). Furthermore, the polymer matrix may sterically hinder the motion of large PF_6^- ions. Reducing polarization by suppressing the anion concentration gradient facilitates lithium ion transport in the proximity of electrodes. The small R_{int} values of the GPE cell (Fig. 7) can be partially attributed to the large t_{Li^+} of GPE. A large t_{Li^+} is beneficial to the rate performance and cycle life of a cell.⁶⁹

3.5. Battery Performance. Fig. 9 shows the galvanostatic charge-discharge profiles of LIBs assembled by inserting the GPE or LE between a graphite anode and a $LiFePO_4$ cathode. This study defined the battery C-rates based on the $LiFePO_4$ cathode by assuming a maximal theoretical capacity of 170 mAh g^{-1} for the full cell system. The battery cells were charged to 3.8 V at 0.1 C and then discharged to 2.0 V at varying discharge rates. At the lowest C-rate (0.1 C) the $LiFePO_4$ -graphite full cells exhibited characteristic charge-discharge plateaus at 3.3 V. The discharge curves deviated from the characteristic equilibrium state curve at high C-rates because fast ion motion resulted in high energy loss. Fig. 10 shows the variation of battery capacity according to C-rates. The capacities of the GPE and LE batteries at 0.1 C were similar (approximately 125 mAh g^{-1}), whereas the GPE battery exhibited much

Huang *et al.*¹⁴

more favorable capacity retention at discharge rates above 7 C. The highest discharge C-rates for the GPE and LE batteries were 20 and 15, respectively. The more favorable rate performance of the GPE battery relative to that of the LE indicated the GPE's lower overall resistance.

The deviation of the discharge voltage plateaus from the equilibrium state, 3.3 V, (i.e., ΔV) corresponded to the sum of the battery's IR drop resulting from the serial resistance and the polarization of the electrodes. The latter was the dominant factor because Fig. 7 reflects that the IR drop (represented as R_b in the equivalent circuit) was much smaller than the polarization of the electrodes (represented by R_{int}). Fig. 11 shows the discharge rate dependence of ΔV for both batteries. The ΔV as a function of the current value displays a linear relationship for the LE battery, and the slope of the straight line yielded a resistance of 93 Ω . The ΔV values of the GPE battery were similar to those of the LE at low discharge rates, but decreased at high discharge rates (> 7 C). The mean slope of the ΔV -against-current in the high-rate region for the GPE battery yielded a resistance of 48 Ω , which was 50% smaller than that of the LE battery. The difference in ΔV for these two batteries indicated that the stabilized SEI formation and large t_{Li^+} value associated with the GPE substantially suppressed the electrode-polarizing tendency at high discharge rates and therefore lowered the resistance caused by polarization. This result explains the more favorable capacity retention of the GPE battery at high C-rates.

To provide a comprehensive perspective on the battery performance, we used the galvanostatic discharge data to correlate the specific power and specific energy of the battery by using the following equations:

$$E = I \int V dt / m \quad (2)$$

$$P = E / \Delta t \quad (3)$$

where E is the specific energy, P is the specific power, I is the discharge current, Δt is the time for complete discharge, and m is the total active material mass of the cathode and anode. Fig. 12 shows a summary of the P and E data in Ragone-type plots. Both the GPE and LE batteries achieved high specific energy values of approximately 210 Wh kg^{-1} . Because of the smaller series resistance at high discharge rates, the GPE battery exhibited a higher attainable power value compared with that of the LE (2.8 kW kg^{-1} vs. 1.3 kW kg^{-1}).

Fig. 13 shows the variation of the discharge capacity based on the number of galvanostatic charge–discharge cycles that occurred between 2.0 and 3.8 V at 1 C-rate. The capacity retention of the GPE battery remained at approximately 100% in the first 200 cycles, and still maintained an impressive retention of 77% after 450 cycles. The LE battery exhibited only 44% capacity retention after 450 cycles. The outstanding cycling performance of the GPE battery can be attributed to the supportive role of the P(EO-co-PO) polymer framework that entrapped a large amount of electrolyte solution to provide free volume for ion motion and specifically facilitated the transport of solvated- Li^+ ions to minimize electrode polarization, which was shown to dominate the energy loss of the batteries (Figs. 7 and 9). This study demonstrated that using the ether-abundant GPE to replace conventional liquid electrolytes that swell commercial separators improved the specific power and cycle life of a full-cell battery and has the potential for further application in flexible devices that require the leak-proof construction and easy fabrication of these devices into desired shapes and sizes.

4. Conclusions

Huang *et al.* 16

Ether-abundant GPE derived from swelling the P(EO-co-PO) copolymer with LE (i.e., 1 M LiPF₆-EC/DMC/DEC) exhibited an ionic conductivity of $3.8 \times 10^{-3} \text{ S cm}^{-1}$ (30 °C), which was higher than that of LE when swelling a commercial separator, and demonstrated structural integrity that is suitable for full-cell LIB assembly. The high solvent-coordinating ability of ether groups in the GPE created free volume for ion motion and facilitated the transport of solvent-solvated Li⁺ ions through the segmental movement of polymer chains. This specific polymer framework led to high ionic conductivity and a high lithium transference number of 0.7 for the GPE, whereas LE, when swelling a separator, exhibited a transference number of 0.4. The GPE exhibited smaller interfacial resistance against lithium metal than the LE did. Incorporating the carbonate solvent molecules into the P(EO-co-PO) polymeric framework may have stabilized the solvent and suppressed the formation of thick SEI layers that hinder interfacial ion transport. Because of the high lithium transference number and low interfacial resistance of the GPE, the graphite|GPE|LiFePO₄ battery outperformed the graphite|LE|LiFePO₄ battery by exhibiting a 50% smaller resistance at high rates (7–20 °C) and double the specific power to achieve 2.8 kW kg⁻¹. The graphite|GPE|LiFePO₄ battery exhibited negligible capacity decay in the first 200 cycles of charge–discharge cycling at 1 C-rate and exhibited an impressive 77% capacity retention after 450 cycles. The aforementioned electrochemical analysis revealed that P(EO-co-PO) represents a promising matrix for GPEs used in high-power and long-cycle-life LIBs; its mechanical integrity and durable structure make the synthesized GPE readily scalable to a roll-to-roll LIB assembly process.

Acknowledgements

This research was supported by the National Science Council of Taiwan (101-2221-E-006-243-MY3, 101-2221-E-006-225-MY3, 102-3113-P-006-012, and 102-3113-E-006-002), the “Aim for the Top-Tier University and Elite Research Center Development Plan” of National Cheng Kung University

† **Electronic Supplementary Information (ESI) available:** Nyquist impedance plots of GPE and LE inserted between two stainless-steel electrodes at various temperatures. See DOI: 10.1039/b000000x/.

References

1. X. Yang, F. Zhang, L. Zhang, T. Zhang, Y. Huang and Y. Chen, *Adv. Funct. Mater.* 2013, **23**, 3353-3360.
2. S. J. Park, K. Yoo, J. Y. Kim, J. Y. Kim, D. K. Lee, B. S. Kim, H. Kim, J. H. Kim, J. Cho and M. J. Ko, *ACS Nano* 2013, **7**, 4050-4056.
3. Y. Zhu, S. Xiao, Y. Shi, Y. Yang, Y. Hou and Y. Wu, *Adv. Energy Mater.* 2014, **4**, DOI: 10.1002/aenm.201300647.
4. C. W. Huang, C. A. Wu, S. S. Hou, P. L. Kuo, C. T. Hsieh and H. Teng, *Adv. Funct. Mater.* 2012, **22**, 4677-4685.
5. M. F. Hsueh, C. W. Huang, C. A. Wu, P. L. Kuo and H. Teng, *J. Phys. Chem. C* 2013, **117**, 16751-16758.
6. J. Cao, L. Wang, M. Fang, Y. Shang, L. Deng, J. Yang, J. Li, H. Chen and X. He, *Electrochim. Acta* 2013, **114**, 527-532.
7. S. S. Hwang, C. G. Cho and H. Kim, *Electrochem. Commun.* 2010, **12**, 916-919.
8. P. Isken, M. Winter, S. Passerini and A. Lex-Balducci, *J. Power Sources* 2013, **225**, 157-162.
9. K. Zaghbi, K. Striebel, A. Guerfi, J. Shim, M. Armand and M. Gauthier, *Electrochim. Acta* 2004, **50**, 263-270.
10. K. Zaghbi, P. Charest, P. Guerfi, J. Shim, M. Perrier and K. Striebel, *J. Power Sources* 2005, **146**, 380-385.
11. Y. Kobayashi, S. Seki, Y. Mita, Y. Ohno, H. Miyashiro, P. Charest, A. Guerfi and K. Zaghbi, *J. Power Sources* 2008, **185**, 542-548.
12. S. Seki, K. Takei, H. Miyashiro and M. Watanabe, *J. Electrochem. Soc.* 2011, **158**, A769-A774.
13. H. Zheng, L. Chai and X. Song, V. Battaglia, *Electrochim. Acta* 2012, **62**,

- 256-262.
14. C. M. Yang, H. S. Kim, B. K. Na, K. S. Kum and B. W. Cho, *J. Power Sources* 2006, **156**, 574-580.
 15. H. Li, Y. M. Chen, X. T. Ma, J. L. Shi, B. K. Zhu and L. P. Zhu, *J. Membr. Sci.* 2011, **379**, 397-402.
 16. X. L. Wang, Q. Cai, L. Z. Fan, T. Hua, T. H. Lin and C. W. Na, *Electrochim. Acta* 2008, **53**, 8001-8007.
 17. G. P. Pandey, R. C. Agrawal and S. A. Hashmi, *J. Power Sources* 2009, **190**, 563-572.
 18. S. Ferrari, E. Quartarone, P. Mustarelli, A. Magistris, M. Fagnoni, S. Protti, C. Gerbaldi and A. Spinella, *J. Power Sources* 2010, **195**, 559-566.
 19. N. Wu, Q. Cao, X. Y. Wang, X. Y. Li and H. Y. Deng, *J. Power Sources* 2011, **196**, 8638-8643.
 20. P. Raghavan, J. Manuel, X. H. Zhao, D. S. Kim, J. H. Ahn and C. W. Nah, *J. Power Sources* 2011, **196**, 6742-6749.
 21. D. Kumar and S. A. Hashmi, *J. Power Sources* 2010, **195**, 5101-5108.
 22. Y. F. Wang, X. Y. Ma, Q. L. Zhang and N. Tian, *J. Membr. Sci.* 2010, **349**, 279-286.
 23. H. R. Jung and W. J. Lee, *Electrochim. Acta* 2011, **58**, 674-680.
 24. B. Scrosati and J. Garche, *J. Power Sources* 2010, **195**, 2419-2430.
 25. K. Zaghib, P. Charest, A. Guerfi, J. Shim, M. Perrier and K. Striebel, *J. Power Sources* 2004, **134**, 124-129.
 26. Q. Lu, J. Fang, J. Yang, R. Miao, J. Wang and Y. Nuli, *J. Membr. Sci.* 2014, **449**, 176-183.

Huang *et al.* 20

27. M. Rao, J. Liu, W. Li, Y. Liang, Y. Liao and Z. Zhao, *J. Power Sources* 2009, **189**, 711-715.
28. N. Oyama, Y. Fujimoto, O. Hatozaki, K. Nakano, K. Maruyama, S. Yamaguchi, K. Nishijima, Y. Iwase and Y. Kutsuwa, *J. Power Sources* 2009, **189**, 315-323.
29. Y. H. Liao, X. P. Li, C. H. Fu, R. Xu, L. Zhou, C. L. Tan, S. J. Hu and W. S. Li, *J. Power Sources* 2011, **196**, 2115-2121.
30. J. Liu, W. Li, X. Zuo, S. Liu and Z. Li, *J. Power Sources* 2013, **226**, 101-106.
31. J. A. Choi, Y. Kang, H. Shim, D. W. Kim, E. Cha and D. W. Kim, *J. Power Sources* 2010, **195**, 6177-6181.
32. J. L. Acosta and E. Morales, *Solid State Ionics* 1996, **85**, 85-90.
33. K. Schillén, J. Jansson and D. Löf, T. Costa, *J. Phys. Chem. B* 2008, **112**, 5551-5562.
34. D. H. Sun, D. X. Sun and Y. Hao, *Mater. Sci. Forum* 2008, **663-665**, 1125-1128.
35. B. Bharatiya, G. Ghosh, P. Bahadur and J. Mata, *J. Dispersion Sci. Technol.* 2008, **29**, 696-701.
36. W. J. Liang, T. Y. Chen and P. L. Kuo, *J. Appl. Polym. Sci.* 2004, **92**, 1264-1270.
37. C. P. Tien, W. J. Liang, P. L. Kuo and H. S. Teng, *Electrochim. Acta* 2008, **53**, 4505-4511.
38. S. Zugmanna, M. Fleischmann, M. Amerellera, R. M. Gschwindb, H. D. Wiemhöferc and H. J. Goresa, *Electrochim. Acta* 2011, **56**, 3926-3933.
39. M. Doyle and T. F. Fuller, J. Newman, *Electrochim. Acta* 1994, **39**, 2073-2081.
40. A. Ghosh, C. Wang and P. Kofinas, *J. Electrochem. Soc.* 2010, **157**, A846-A849.
41. B. Beak, F. Xua and C. Jung, *Solid State Ionics* 2011, **202**, 40-44.
42. P. Verma, P. Maire and P. Novák, *Electrochim. Acta* 2010, **55**, 6332-6341.
43. M. Nie, D. P. Abraham, D. M. Seo, Y. Chen, A. Bose and B. L. Lucht, *J. Phys.*

- Chem. C* 2013, **117**, 25381-25389.
44. K. Ui, D. Fujii, Y. Niwata, T. Karouji, Y. Shibata, Y. Kadoma, K. Shimada and N. Kumagai, *J. Power Sources* 2014, **247**, 981-990.
45. S. S. Zhang, *J. Power Sources* 2007, **164**, 351-364.
46. T. Shodai, B. B. Owens, H. Ohtsuka and J. I. Yamaki, *J. Electrochem. Soc.* 1994, **141**, 2978-2981.
47. J. V. Gulmine, P. R. Janissek, H. M. Heise and L. Akcelrud, *Polym. Test* 2002, **21**, 557-563.
48. P. He, Y. Xiao, P. M. Zang, C. H. Xing, N. Zhu, X. Y. Zhua and D. Y. Yan, *Polym. Degrad. Stabil.* 2005, **88**, 473-479.
49. P. Moonsri, R. Watanesk, S. Watanesk, H. Niamsup and R. L. Deming, *J. Appl. Polym. Sci.* 2008, **108**, 1402-1406.
50. Y. Ngono, Y. Mare'chal and N. Mermilliod, *J. Phys. Chem. B* 1999, **103**, 4979-4985.
51. D. Luo, Y. Li and M. Yang, *Mater. Chem. Phys.* 2011, **125**, 231-235.
52. S. W. Choi, J. R. Kim, S. M. Jo, W. S. Lee and Y. R. Kim, *J. Electrochem. Soc.* 2005, **152**, A989-A995.
53. S. N. Mohamed, N. A. Johari, A. M. M. Ali, M. K. Harun and M. Z. A. Yahya, *J. Power Sources* 2008, **183**, 351-354.
54. R. Aroca, M. Nazri, G. A. Nazri, A. J. Camargo and M. Trsic, *J. Solut. Chem.* 2000, **29**, 1047-1060.
55. K. Kondo, M. Sano, A. Hiwara, T. Omi, M. Fujita, A. Kuwae, M. Iida, K. Mogi and H. Yokoyama, *J. Phys. Chem. B* 2000, **104**, 5040-5044.
56. C. M. Burba and R. Frech, *J. Phys. Chem. B* 2005, **109**, 15161-15164.
57. P. L. Kuo, W. J. Liang and T. Y. Chen, *Polymer* 2003, **44**, 2957-2964.

Huang *et al.*²²

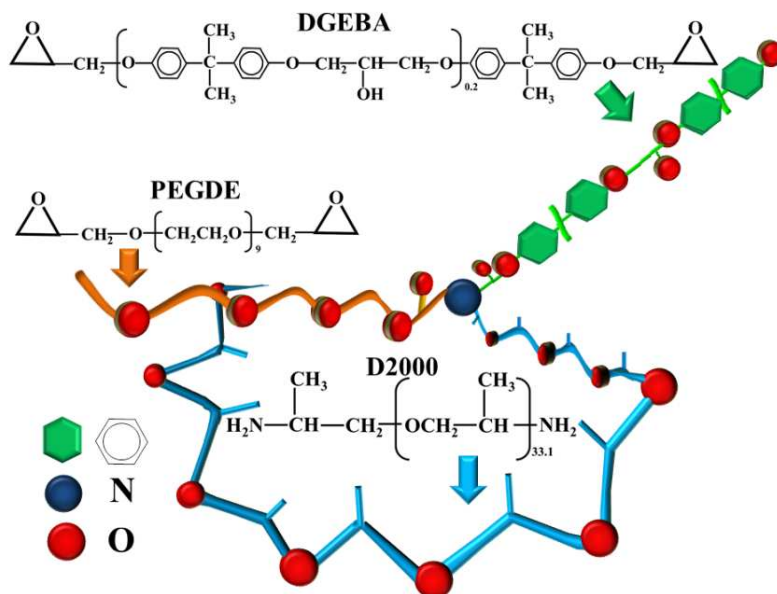
58. M. H. Cohen and D. Turnbull, *J. Chem. Phys.* 1959, **31**, 1164-1169.
59. J. Saunier, F. Alloin, J. Y. Sanchez and G. Caillon, *J. Power Sources* 2003, **119-121**, 454-459.
60. P. G. Bruce, *Solid State Electrochemistry*, Cambridge University Press, United Kingdom, 1997, pp. 98.
61. T. Zhang, N. Imanishi, S. Hasegawa, A. Hirano, J. Xie, Y. Takeda and O. Yamamoto, N. Sammes, *J. Electrochem. Soc.* 2008, **155**, A965-A969.
62. G. B. Appetecchi, F. Croce, G. Dautzenberg, M. Mastragostino, F. Ronci, B. Scrosati, F. Soavi, A. Zanelli, F. Alessandrini and P. P. Prosini, *J. Electrochem. Soc.* 1998, **145**, 4126-4132.
63. H. Y. Sun, Y. Takeda, N. Imanishi, O. Yamamoto and H. J. Sohn, *J. Electrochem. Soc.* 2000, **147**, 2462-2467.
64. S. Liu, N. Imanishi, T. Zhang, A. Hirano, Y. Takeda, O. Yamamoto and J. Yang, *J. Electrochem. Soc.* 2010, **157**, A1092-A1098.
65. S. H. Wang, S. S. Hou, P. L. Kuo and H. Teng, *ACS Appl. Mater. Interfaces* 2013, **5**, 8477-8485.
66. J. Evans, C. A. Vincent and P. G. Bruce, *Polymer* 1987, **28**, 2324-2328.
67. S. Zugmann, M. Fleischmann, M. Amereller, R. M. Gschwind, H. D. Wiemhöfer and H. J. Gores, *Electrochim. Acta.* 2011, **56**, 3926-3933.
68. P. G. Bruce and C. A. Vincent, *J. Electroanal. Chem.* 1987, **225**, 1-17.
69. J. Y. Song, Y. Y. Wang and C. C. Wan, *J. Power Sources* 1999, **77**, 183-197.

Table 1. Capacity Values and Cycle Lives of Full-Cell Lithium Ion Batteries Assembled with LiFePO₄|Graphite Electrodes and Different Electrolytes.

Electrolyte composition (polymer/electrolyte) ^a	Cathode anode ^b	Capacity (mA h g ⁻¹)	Cycling retention (%)	ref.
OEGMA-BnMA/LiPF ₆ -EC-DMC	LFP Graphite	122 @ 0.1C 25 @ 5 C	91%-50 cycles, 0.5 C	8
EO-based/LiBF ₄ -EC-GBL	LFP Graphite	111 @ 1/24 C	80%-180 cycles, 0.5 C	9
EO-based/LiFSI-EC-GBL	LFP Graphite	156 @ 0.04 C	97%-100 cycles, 0.5 C	10
P(EO-MEEGE)/LiTFSI-AN	LFP Graphite	127 @ 1/24 C	64%-80 cycles, 1/16 C	11
----/TG-LiFSI (Liquid phase)	LFP Graphite	107 @ 0.05 C 100 @ 0.4 C	82%-50 cycles, 0.1 C	12
----/LiPF ₆ -EC-DEC (Liquid phase)	LFP MCMB	---	91%-100 cycles, 1 C 68%-500 cycles, 1 C 39%-1000 cycles, 1 C	13
P(EO-PO)/LiPF ₆ -EC-DMC-DEC	LFP Graphite	125 @ 0.5 C 88 @ 5 C 12 @ 17 C	100%-200 cycles, 1 C 77%-450 cycles, 1 C	this work

^aOEGMA-BnMA, oligo(ethylene glycol) methyl ether methacrylate-benzyl methacrylate copolymer; LiPF₆, lithium hexafluorophosphate; EC, ethylene carbonate; DMC, dimethyl carbonate; P(EO/MEEGE), polyethylene oxide-co-2-(2-methoxyethoxy)ethyl glycidyl ether; LiTFSI, lithium bis(trifluoromethylsulfonyl) imide; AN, acetonitrile; LiFSI, lithium bis(fluorosulfonyl) imide; GBL, γ -butyrolactone; LiBF₄, lithium tetrafluoroborate; DEC, diethyl carbonate; TG, triglyme

^bLFP, LiFePO₄; MCMB, mesocarbon microbeads.

Huang *et al.*24

Scheme 1. Conceptual structure of the ether-abundant P(EO-*co*-PO) polymer framework, in which nitrogen atoms connect the PEGDE, DGEBA, and D2000 chains.

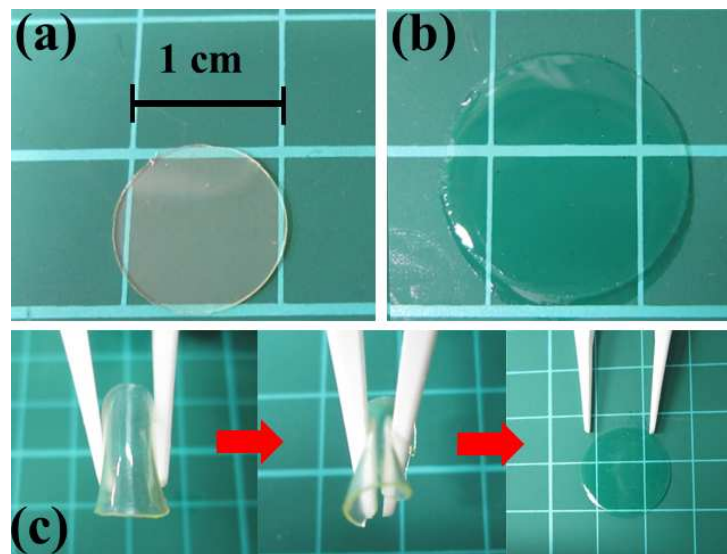


Fig. 1. Top-view photographs: (a) the P(EO-*co*-PO) film; (b) the GPE film that was obtained by soaking the P(EO-*co*-PO) film in the LE solution (1M LiPF₆-EC/DMC/DEC); (c) the GPE film that was bended, twisted, and released to regain its original configuration.

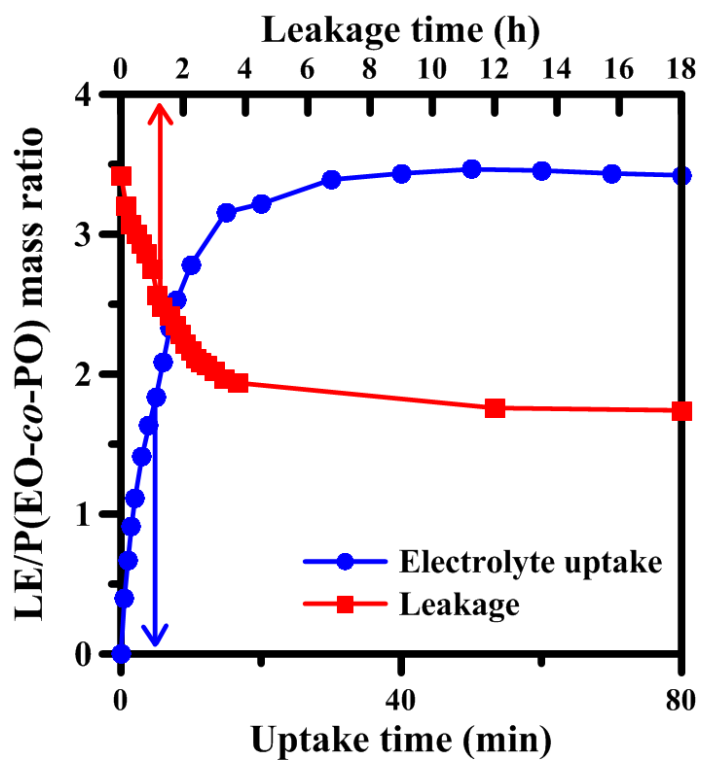


Fig. 2. LE-uptake behavior when soaking the P(EO-co-PO) film in the LE solution (1M LiPF₆-EC/DMC/DEC). The LE uptake reached a saturation value of 3.4 times the polymer film mass in 30 min.

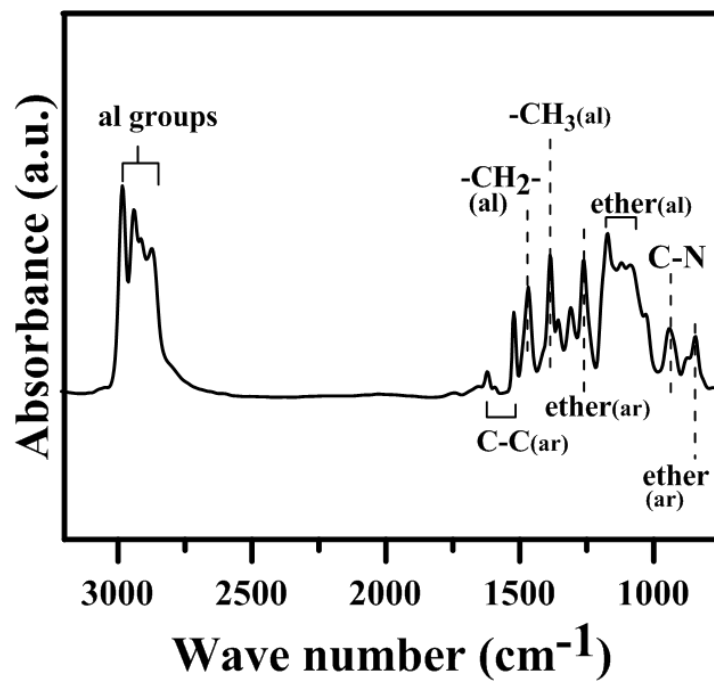


Fig. 3. FTIR absorption spectra of the P(EO-co-PO) film. The symbols al and ar stand for alkyl and aromatic, respectively.

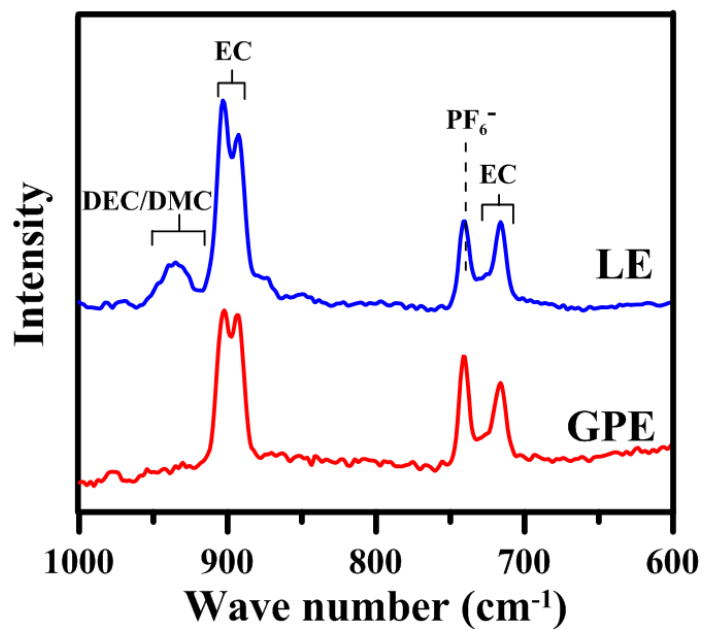


Fig. 4. Raman spectra of LE and GPE in the region of 600–1000 cm⁻¹.

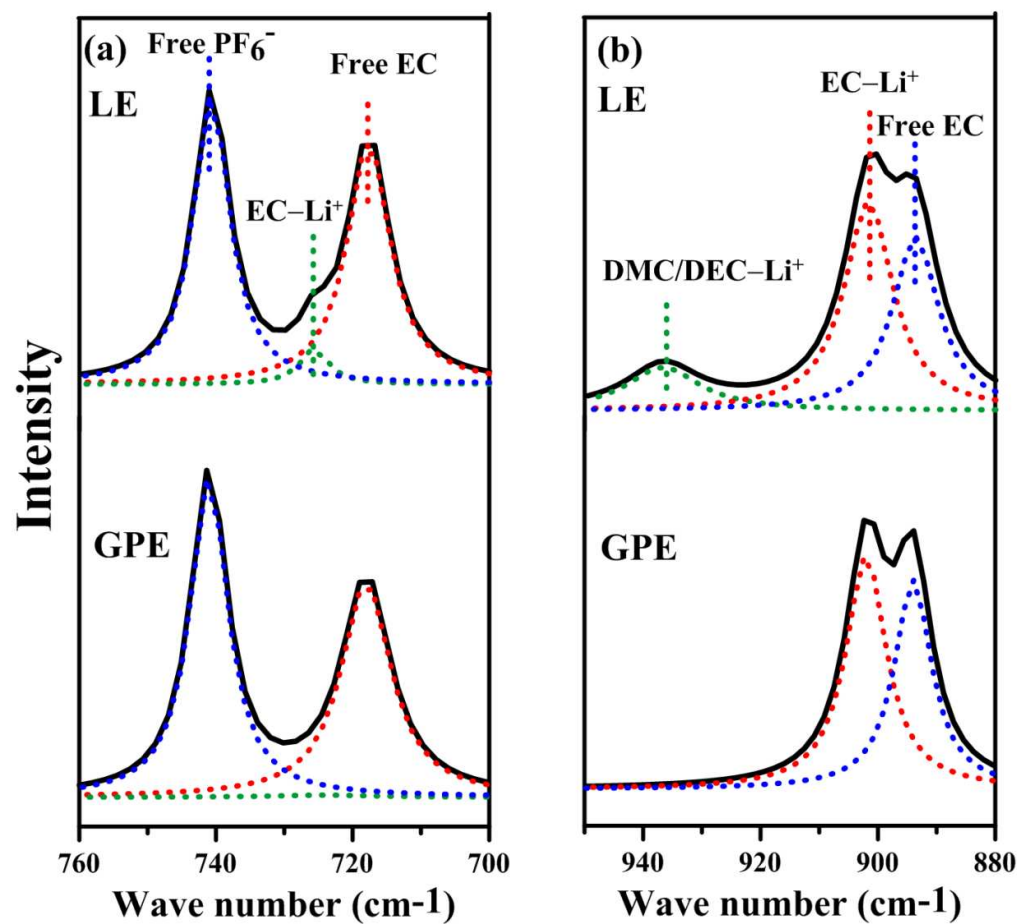


Fig. 5. Raman spectra (solid lines) of LE and GPE and the constituting peaks obtained after spectrum de-convolution (dotted lines) in difference wave-number regimes: (a) 700–760 cm⁻¹ and (b) 880–950 cm⁻¹.

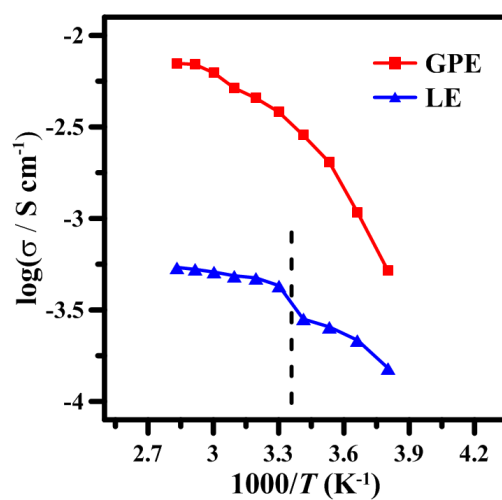


Fig. 6. Nyquist impedance plots of (a) GPE and (b) LE inserted between two stainless-steel electrodes with a frequency range of 0.1 Hz to 1 MHz at 0 V and temperatures of -20–80 °C. Ionic conductivities of the GPE and LE determined from the impedance analysis at temperatures of -20–80 °C (see Fig. S1 of the ESI†).

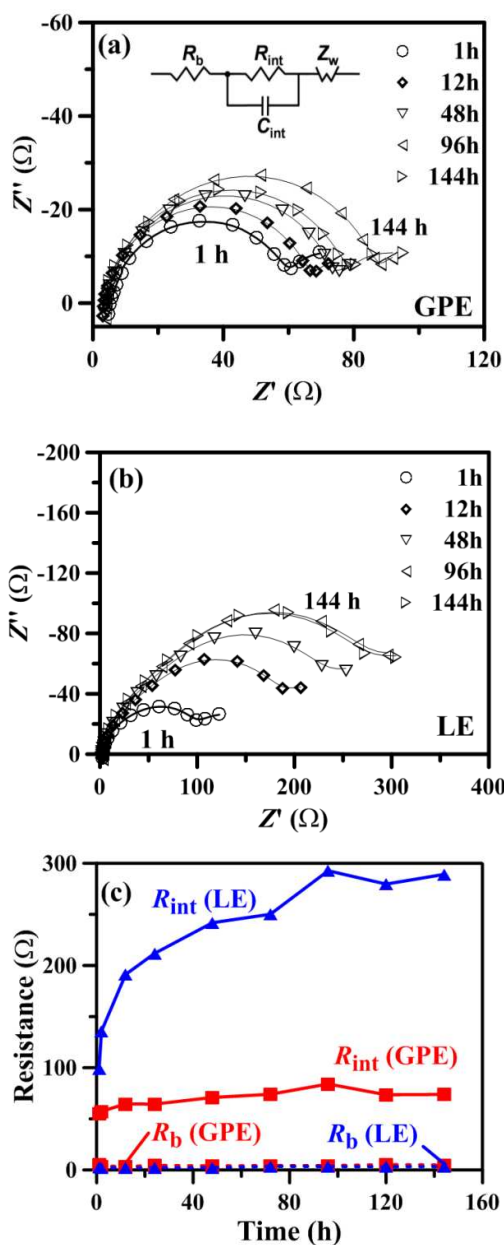


Fig. 7. Nyquist impedance plots of different electrolytes using the sandwich-type Li|electrolyte|Li cell: (a) GPE; (b) LE. The inset in panel a shows the equivalent circuit used for fitting the impedance data, where R_b is the bulk solution resistance, R_{int} is the interface resistance, C_{int} is the interface capacitance, and Z_w is the Warburg impedance element. Panel c shows a summary of the R_b and R_{int} element quantities of the two cells. The measurements were performed with a frequency range of 0.1 Hz to

Huang *et al.*³²

1 MHz at 0 V and 25 °C. The active area of each Li electrode was 1.77 cm². Since the Li/Li⁺ redox reaction was fast, the semicircle associated with this charge transfer process would be negligible. Therefore, each spectra in panels a and b exhibited only one semicircle.

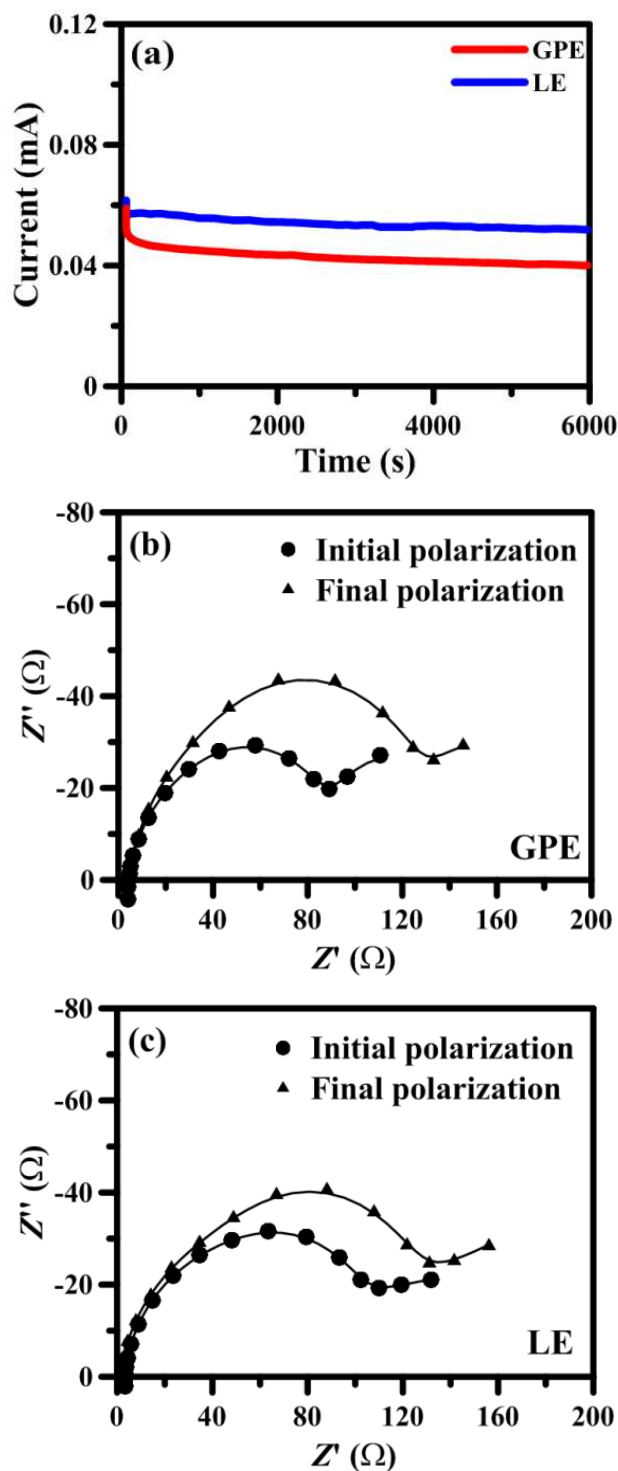


Fig. 8. (a) Current-time curves of the Li|GPE|Li and Li|LE|Li cells after applying a DC voltage of 5 mV to the cell. Corresponding Nyquist impedance plots of the cells for determining the initial and final R_{int} values: (b) GPE; (c) LE. The active area of each Li electrode was 1.77 cm².

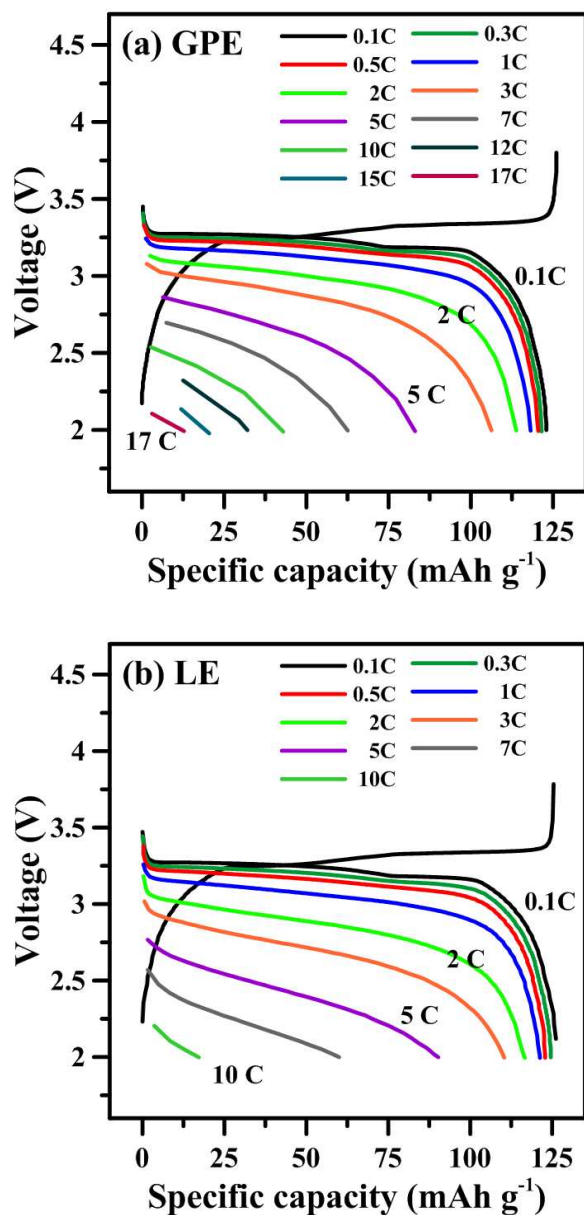


Fig. 9. Galvanostatic charge-discharge profiles of batteries (a) graphite|GPE|LiFePO₄ and (b) graphite|LE|LiFePO₄ at various C-rates between 2.0 and 3.8 V. This study assumes a maximal theoretical capacity of 170 mAh g^{-1} for the LiFePO₄ electrode.

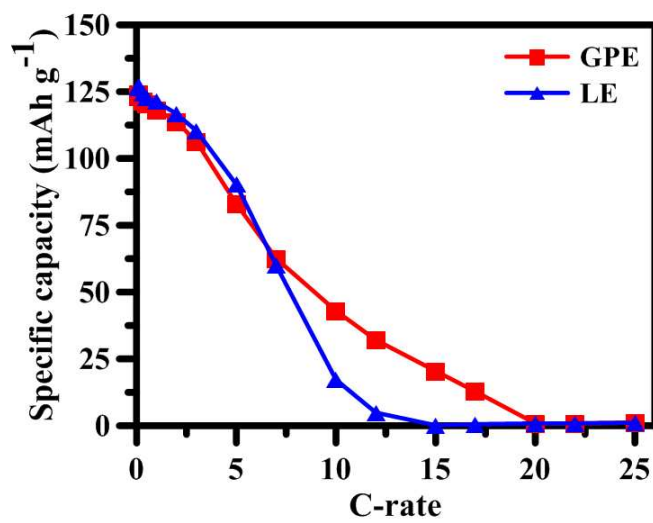


Fig. 10. Discharge capacities of the graphite|GPE|LiFePO₄ and graphite|LE|LiFePO₄ batteries in a series of galvanostatic charge-discharge cycles at various C-rates

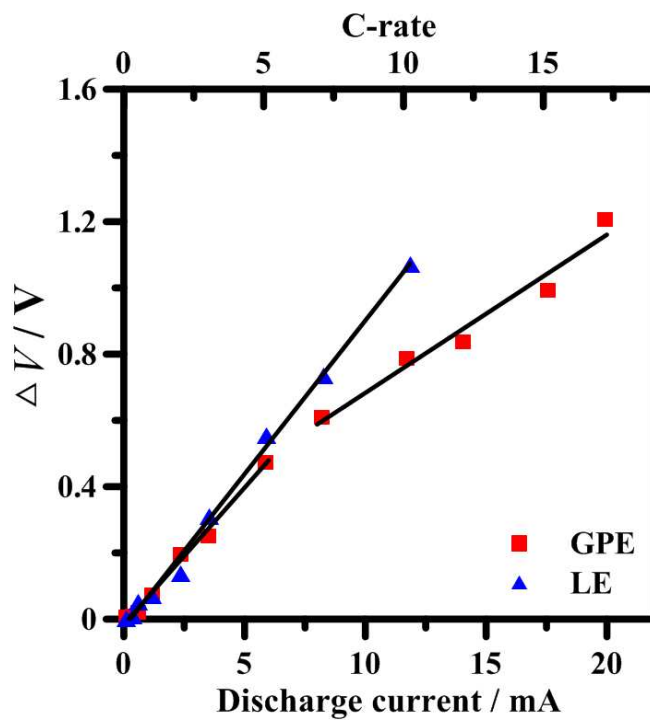


Fig. 11. The deviation of the discharge voltage plateaus from the equilibrium state, 3.3 V, (i.e., ΔV) as a function of the discharge current for the graphite|GPE|LiFePO₄ and graphite|LE|LiFePO₄ batteries. The ΔV value corresponds to the sum of the battery's IR drop resulting from the serial resistance and the polarization of the electrodes.

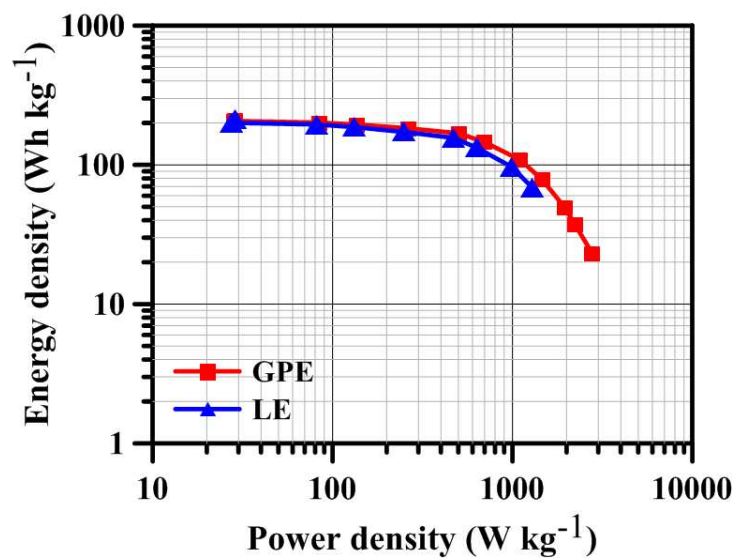


Fig. 12. Ragone plots of the graphite|GPE|LiFePO₄ and graphite|LE|LiFePO₄ batteries. Data obtained from the galvanostatic discharge measurement at various C-rates.

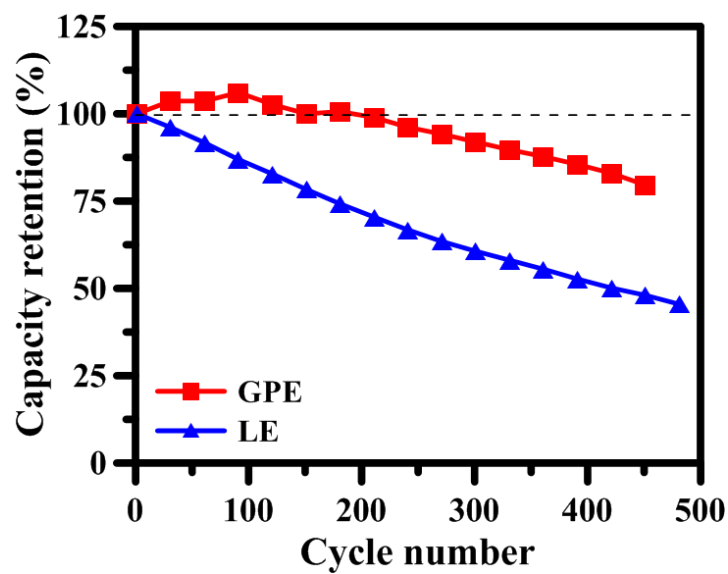


Fig. 13. Discharge capacities of the graphite|GPE|LiFePO₄ and graphite|LE|LiFePO₄ batteries as a function of cycle number at 1C-rate with a voltage range between 2.0 and 3.8 V.

Table of contents entry:

P(EO-co-PO) with high solvent-entrapping ability represents a promising matrix for GPEs used in high-rate and long-cycle-life lithium ion batteries.

